Hindawi
International Journal of Chemical Engineering
Volume 2023, Article ID 9826309, 1 page
https://doi.org/10.1155/2023/9826309

*Retraction*

# Retracted: Photocatalytic Performance Study of Organophosphorus-Doped Tungsten Trioxide and Composite Materials

**International Journal of Chemical Engineering**

Received 17 October 2023; Accepted 17 October 2023; Published 18 October 2023



This article has been retracted by Hindawi following an investigation undertaken by the publisher [1]. This investigation has uncovered evidence of one or more of the following indicators of systematic manipulation of the publication process:

(1) Discrepancies in scope
(2) Discrepancies in the description of the research reported
(3) Discrepancies between the availability of data and the research described
(4) Inappropriate citations
(5) Incoherent, meaningless and/or irrelevant content included in the article
(6) Peer-review manipulation

The presence of these indicators undermines our confidence in the integrity of the article's content and we cannot, therefore, vouch for its reliability. Please note that this notice is intended solely to alert readers that the content of this article is unreliable. We have not investigated whether authors were aware of or involved in the systematic manipulation of the publication process.

Wiley and Hindawi regrets that the usual quality checks did not identify these issues before publication and have since put additional measures in place to safeguard research integrity.

We wish to credit our own Research Integrity and Research Publishing teams and anonymous and named external researchers and research integrity experts for contributing to this investigation.

The corresponding author, as the representative of all authors, has been given the opportunity to register their agreement or disagreement to this retraction. We have kept a record of any response received.

## References

[1] P. Zhang, J. Sun, Q. wang, W. Chen, and X. Li, "Photocatalytic Performance Study of Organophosphorus-Doped Tungsten Trioxide and Composite Materials," *International Journal of Chemical Engineering*, vol. 2022, Article ID 5040439, 8 pages, 2022.

Hindawi
International Journal of Chemical Engineering
Volume 2022, Article ID 5040439, 8 pages
https://doi.org/10.1155/2022/5040439



*Research Article*

# Photocatalytic Performance Study of Organophosphorus-Doped Tungsten Trioxide and Composite Materials

**Ping Zhang**,[1,2] **Jiayu Sun**,[2] **Qi wang**,[2] **Wei Chen**,[1] **and Xiaochen Li**[2]

[1]*College of Environment, Hohai University, Nanjing 210098, China*
[2]*College of Water Conservancy and Civil Engineering, Shandong Agricultural University, Tai'an 271000, China*

Correspondence should be addressed to Ping Zhang; 19402454@masu.edu.cn

Received 7 July 2022; Revised 1 August 2022; Accepted 8 August 2022; Published 24 August 2022

Academic Editor: G.L. Balaji



The present study successfully produced a highly effective and stable organ phosphorus-doped tungsten trioxide (P-$WO_3$) photocatalyst by a combination of hydrothermal and postcalcination methods. The crystallites, morphologies, and optical properties of the produced $WO_3$ and P-$WO_3$ crystals were investigated. The results indicated that P was consistently doped into the $WO_3$ lattice in a pentavalent-oxidation state (P5+). Additionally, charge carrier traps capable of accepting photoelectrons were created. Additionally, the optical band gap was reduced from 2.4 to 2.33 eV. The degradation of methyl blue by photocatalysts was utilized to evaluate the photocatalytic performance of the synthesized P-$WO_3$ samples at varied P concentrations (MB). The sample containing 6% -P-$WO_3$ exhibited the best photocatalytic performance, degrading 96 percent of MB in 120 minutes, which was more than four times faster than the pure $WO_3$ sample. The practicality of the synthesized P-$WO_3$ was determined using samples from two residential wastewater treatment plants. When treating real wastewater with low organic matter concentrations, the P-$WO_3$ demonstrated strong photodegradation performance. The creation of hydroxyl radicals (OH) and photography-created holes (h+) could be the key protagonists of photocatalytic activity in the P-$WO_3$.

## 1. Introduction

Tungsten has a higher heat capacity (3410°C) and thickness (19.3 g $cm^3$) comparable to g (19.32 g $cm^3$). Tungsten's crystallographic partner controllable state (grid boundary: 0.3165 nm) is -W (grid type: body-jogged shape). -W is a cubic (type A15) crystallite of tungsten that was discovered during hydrogen reduction. $WO_3$-W is a tungsten FCC form found only in thin films. Tungsten is frequently utilized in refractory alloys due to its unique attributes. W-based heterogeneous catalysts are composed of tungsten oxides, sulfides, carbides, or heteropolytungstates, whereas group 8-11 elements are currently being used in catalysis as non-material elements. Tungsten hydrides, therefore less commonly used than molybdenum salts, are necessary factors for hydrotreating catalysts. More recently, tungsten sulphide-based catalysts and photocatalysts have been created for use in hydrogen production via water splitting. In the field of hydrogen evolution reaction, tungsten carbides are used in electrochemical applications [1, 1]. Heteropolytungstates are used as tungsten precursors in the creation of W-based catalysts because of their high-water solubility. They are also used in a variety of organic reactions, including oxidation reactions. Heteropolytungstates, which are associated with metals such as cobalt, are also effective water-splitting catalysts.

Tungsten trioxide ($WO_3$) is a by and large dark semiconductor that may be established by visible light (450 nm), making it a better semiconductor for decreasing VOCs in an indoor environment [2,3]. Various strategies for the combination of $WO_3$ nanostructures have been recorded, including substance fume statement (CVD), warm vanishing, electrochemical methods, a shower pyrolysis approach, format intervened union, the sol-gel methodology, and aqueous processes. In conclusion, unidirectional composites have the same form as conventional materials in terms of the stress-strain relations that control the stiffness of all materials. There are no extra phrases or more intricate relationships.

There is only one difference: there are four independent constants for composites as opposed to two for normal materials. However, there are no conceptual or practical obstacles that would make working with composites difficult by nature. Actually, once we comprehend composites, we will naturally comprehend ordinary materials as unique instances of composites[4].

*1.1. Tungsten-Based Catalysis Design.* Tungsten trioxide ($WO_3$) is a generally obscure semiconductor that can be activated by visible light (450 nm), making it a better semiconductor for reducing VOCs in an indoor environment. Various strategies for the combination of $WO_3$ nanostructures have been recorded, including substance fume statement (CVD), warm vanishing, electrochemical methods, a shower pyrolysis approach, format intervened union, the sol-gel methodology, and aqueous.

*1.2. Tungsten Trioxide.* There are various possible allotropic forms of tungsten trioxide, including two monoclinic structures (−$WO_3$ and −$WO_3$), an FCC crystal structure (-$WO_3$), and a hexagonal structure (h-$WO_3$). Corner-sharing octahedra of $WO_6$ units make up all of these $WO_3$ forms. The octahedra are arranged in a quasicubic pattern by the monoclinic and triclinic structures. The angles of bending between adjacent octahedra distinguish them [6–6]. Only at low temperatures (T 17°C) is triclinic $WO_3$ stable. The ideal cubic framework of WO6 blocks, according to ab initio calculations, is not stable and has a tendency to take on a tetragonal shape [7–11]. Recently, Sun et al. investigated the electrochemical and gas adsorption properties of monoclinic $WO_3$ (m-$WO_3$) and hexagonal $WO_3$ (h-$WO_3$). Figure 1 shows tungsten trioxide.

## 2. $WO_3$ Nanostructured

Semiconductor nano-structured creation and controlled growth is a fast-growing new discipline in the chemistry of materials. Much of this study has focused on quantum confinement phenomena in optically active IIVI and III-V semiconductors. Indeed, the size and shape of the colour-coordinated nanoparticles significantly influence the optical and electrical properties of the last option compounds [12]. Subsequently, it is important to deal with the shape and size dissemination of semiconductor nanoparticles for effective utilization in light-emitting diodes and biological labelling. Studies on oxide semiconductor nanostructures, on the other hand, are predominately focused on the creation of higher specific, mesoporous, transparency films for use in photovoltaic panels and picture catalytic.

*2.1. Properties.* The formation and morphology of a material have a major effect on its visual aspects. Different film preparation procedures have distinct properties for a variety of applications. There are advantages in terms of film quality and material production costs [13]. Amorphous (−$WO_3$) and crystalline (−$WO_3$) are the two structural orders of

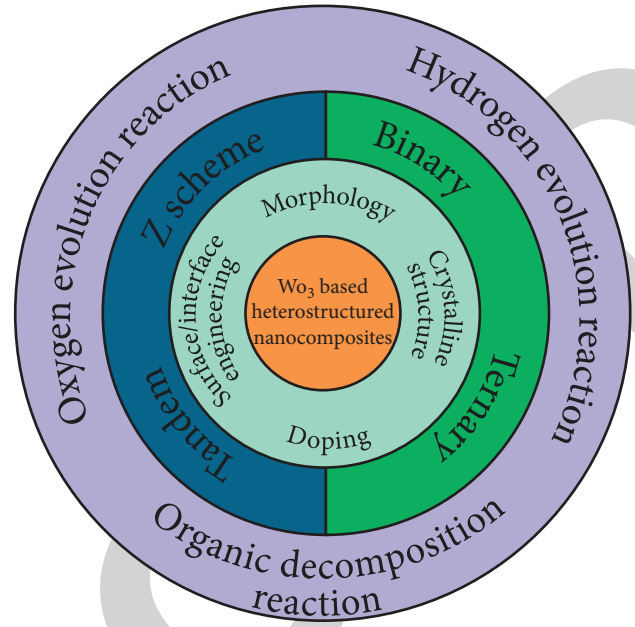


Figure 1: Tungsten trioxide.

tungsten oxide thin films (c-$WO_3$). The distorted rhenium trioxide ($ReO_3$) structure is the $WO_3$ crystal lattice's architectural design. Although tungsten oxide was an excellent candidate for photochromic devices, it is not widely used due to the rapid advancements in fluid gem shows (LCDs). Presently, tungsten oxide films are utilized in shades, vehicle back view mirrors, solar rooftops, and configuration string windows for auto and commercial applications creating glass. Figure 2 shows the crystal structure of monoclinic $WO_3$.

*2.2. Applications.* In everyday life, tungsten trioxide is designed for a diverse array of applications. It is oftentimes utilized in industries to make tungsten for x-pillar screens, photoluminescence, heat-evidence surfaces, and gas sensors. In view of its brilliant yellow tone, $WO_3$ is typically used as a shade in pottery and paints. Tungsten trioxide has of late been utilized to manufacture electrically chromic window frames, sometimes known as smart windows. Electrically switchable glass is used in these windows, which alters the light transmission qualities when a voltage is applied [14, 17]. This enables the user's windows to be tinted to control how much heat or radiation passes through. Tungsten oxide is a promising inorganic material with excellent electrochromic, photochromic, and gas-chromic properties. It has been studied for use in electrochromic, gas-chromic, solar energy, optical signal transduction, and posting [18, 19]. Other software, optical gadgets, level board shows, and gas, dampness, and temperature sensors are also incorporated. $TiO_2$ is a stylishly satisfying material with phenomenal photograph-responsive properties, and a few specialists have endeavored to upgrade the hue execution of $WO_3$ dainty movies by doping $TiO_2$.The overwhelming majority of $WO_3/TiO_2$ research has focused on composite

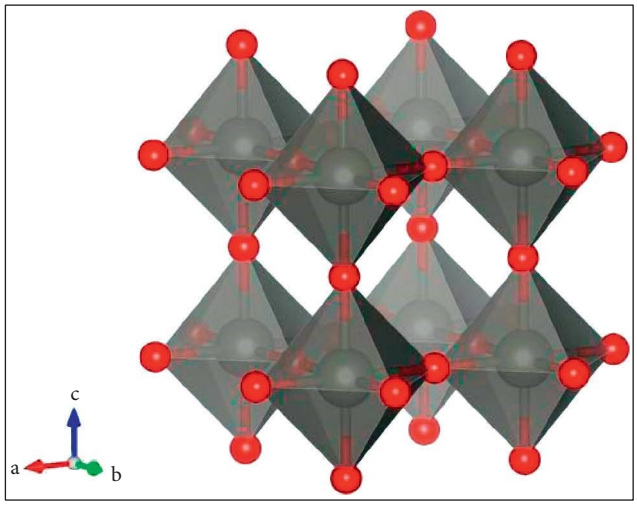


Figure 2: Crystal structure of monoclinic $WO_3$.

thin films. Figure 3 shows $WO_3/TiO_2$ composite film formations.

## 3. Methodology

ICP-AES investigation revealed that $WO_3$ particles created from the slick tungstic corrosive forerunner (i.e., W0) have a sodium nuclear centralization of 2.78 104 for every iota of W. Because of the way that the beginning arrangement contains two particles of Na for each one molecule of W, the extensive fall in fixation proposes a high evacuation proficiency through the particle trade process [13, 14]. The W0 particles had a yellow covering and were believed to be a mix of the monoclinic $WO_3$ stage (cell constants: a = 7.2970, b = 7.5390, c = 7.6880; JCPDS 01-071-2141) and the orthorhombic $WO_3{\cdot}13H_2O$ stage (cell constants: a = 7.3590, b = 12.5130, c = 7.7040; JCPDS 00-035-0270). The stage blend in W0 is consistent with the parchedness advancement profile of tungstic corrosive portrayed by Livage and Guzman.

WSA is composed of nanoparticles ranging in size from 30 to 100 nm and was discovered to have a pure monoclinic crystalline phase by XRD.

*3.1. Effect of Sulphate Anions and pH on $WO_3$ Characteristics.* Figure 1 B and C show the effect of sulfate (got from Na2SO4) as a shape-putting together master on the morphology of $WO_3$ for W0.3NaS and W7.6NaS, separately. When contrasted with W0, the two examples display more prolonged structures. The W0.3NaS particles are basically made from aimlessly arranged columnar diamonds, as well as individual particles, while the W7.6NaS particles are made from packaged nanorods [17]. The variety in morphology can be traced for the most part to the expansion of SO4 2 anions, as the last arrangements had equivalent pH values. Notably, the SO4 2 anions incite an anisotropic turn of events. One way shape-controlling added substances can act is by "covering" molecule improvement along a specific gem plane. A total of preframed nanorods by means of coordinated connection might be enthusiastically beneficial to limit the system's surface energy, and thus, nanorod $WO_3$ bundles are created for W7.6NaS. Figure 4 shows selected synthesis parameters and characteristics for the different $WO_3$.

Using varying concentrations of the sulfate expansion in aqueous amalgamation can bring about the development of particular $WO_3$ glasslike stages. Whenever the $SO_4$ 2/$WO_4$ 2 proportion was diminished to W0.3NaS, XRD revealed that the translucent stage was indistinguishable from W0. This revelation infers that the sulfate expansion is basic not just for changing the morphology of the item but additionally for controlling its translucent stage. Gu et al. [17] further determined the significance of sulfate salt expansion in affecting the translucent period of the $WO_3$ item. It has been seen that as many sulfate antacid metal salts are expanded, the hexagonal stage at last becomes prevalent, which concurs with our outcome [21]. Albeit the sodium particles in the $Na_2SO_4$-added substance taken out during the particle trade process, it is conceivable that some Na + particles stayed in the forerunner arrangement (W7.6NaS, in particular, has a lot higher Na2SO4 focus) and went about as settling particles for the hexagonal and three-sided burrows during the development of metastable hexagonal $WO_3$.

*3.2. Pt/$WO_3$ Characteristics.* When UV-An and visible light were used, the photo deposition of Pt on $WO_3$ nanocubes (W7.6HS) was more visible. In the two cases, the Pt stores are hemispherical and have a particular person, with the photographed statement under UV-A light seeming to expand the event of more modest (2-3 nm) stockpiling. While noticeable light photodeposition leaned toward Pt stores in the 5-10 nm range, UV light photodeposition created some bigger Pt stores (10 nm). The WSA test yielded the most indisputable outcomes. Articulated change in Pt photodeposit properties occurred because of the different light sources [22]. Pt photodeposition on WSA involving noticeable light leads to the gathering of groups of minuscule Pt stores on the $WO_3$ spherical particles. The Pt nanoparticles held inside the bundles seem, by all accounts, to be somewhere in the range of 2 and 3 nm in size, with the genuine gatherings estimated at roughly 20 nm in expansiveness. Individual Pt stores seem, by all accounts, to be accessible on the $WO_3$ particles too. The TEM pictures show that the different $WO_3$ estimations and light frequencies impact the Pt photodeposition cycle.

The valence condition of the stored platinum nanoparticles is critical for charge capturing and interfacial charge transfer, as well as for the platinized metal oxide's photocatalytic capability. The range can be deconvoluted into two sets of doublets based on the platinum oxidation state. The principal sets of doublets were assigned to the nuclear state Pt0, whereas the second sets of doublets were assigned to the oxidation provinces of Pt. The standardized pinnacle locales were determined by contrasting the dominant species in both UV-An and apparent light photodeposition [23]. In spite of the fact that we utilized noticeable light (3 h) for photodeposition of platinum on $WO_3$ upholds,

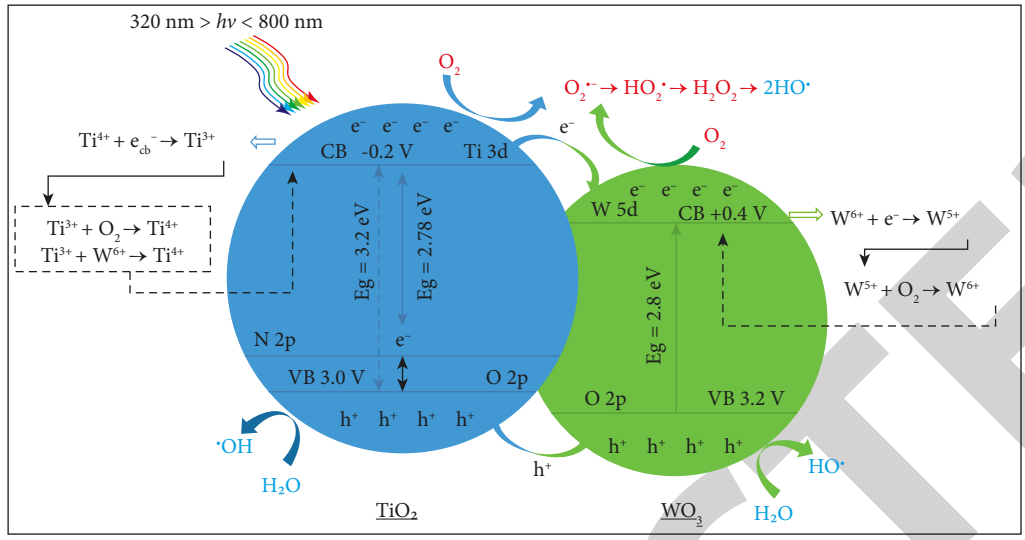


Figure 3: $WO_3/TiO_2$ composite film formations.

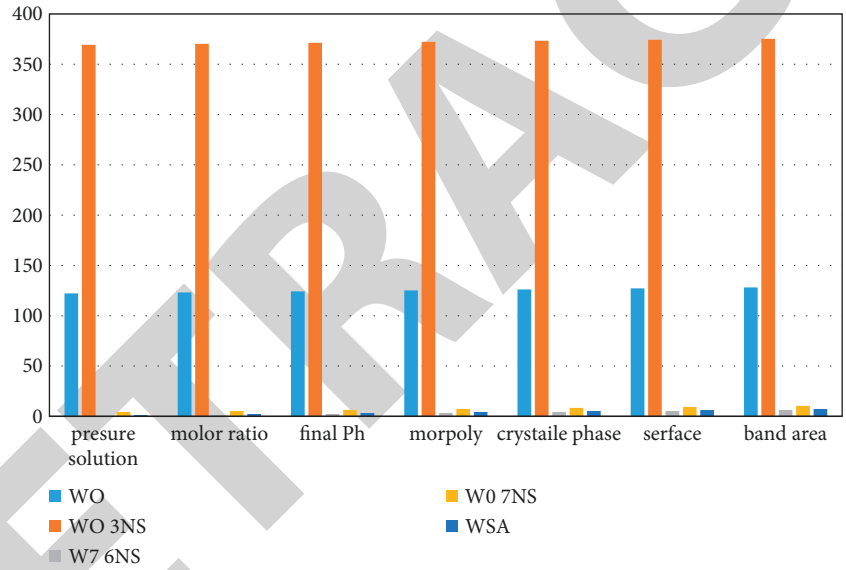


Figure 4: Selected synthesis parameters and characteristics for the different $WO_3$ photocatalysts. Included are the characteristics of commercial Sigma Aldrich $WO_3$ (WSA).

we cannot preclude the likelihood that the aggregate sum of photons from the apparent light enlightenment was lacking to lessen the Pt antecedent to Pt metal.

XPS spectra of platinum were photodeposited on $WO_3$ nanocubes (W7.6HS) with (*A*) UV-A light for 60 minutes and (B) visible light for 3 hours. Figure 5 shows UV-A light for 60 minutes, and Figure 6 shows apparent light for 3 hours.

*3.3. Photo Catalytic Studies.* In a 0.25 L conical flask, 1 g of the nanomaterials was acquainted with 0.1 L of nearby coloring gushing preceding photocatalytic tests. For 6 hours, the blend was mixed at 150 rpm in obscurity without daylight, utilizing an attractive stirrer. The assessment was focused on standard time spans h, and the models were then tried for TOC and COD. This was done to conclude the uttermost adsorption spans of the as of late made nanomaterials. Once more, 0.1 L of the colouring wastewater was added into a 0.25 L cone-shaped carafe and then exposed to direct sunlight for 6 hours while being blended at 150 rpm using an attractive stirrer. The examination was conducted over a period of time, and the TOC and COD were not set in stone [24]. This was done to exhibit that the percent evacuation or mineralization of natural colours in nearby colouring profluent at surrounding temperature was no doubt inferable from photolysis and not to photocatalysis or adsorption by the nanomaterials. The photocatalytic tests were finished in a 0.5 L changed photograph reactor with 0.1 L of neighborhood assortment wastewater containing 1 g of $WO_3$ nanoparticles. Following that, to guarantee that the colour atoms had arrived at their adsorption-desorption

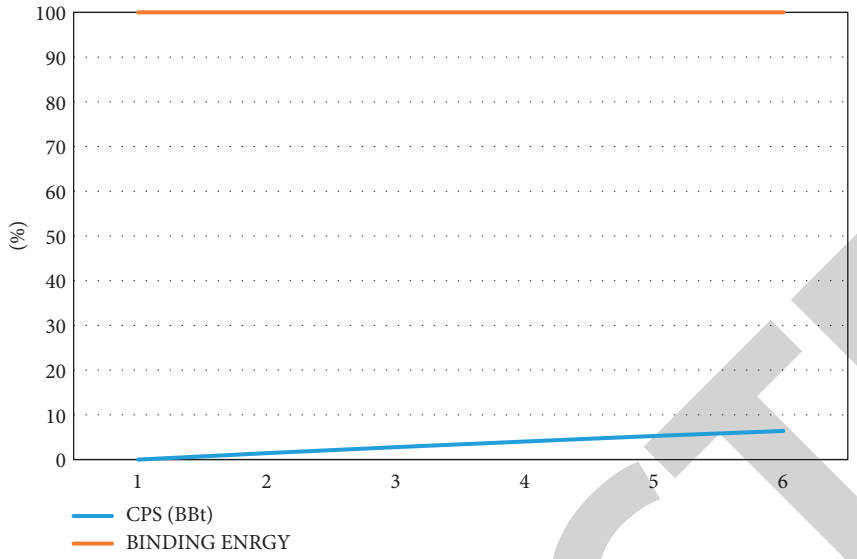


Figure 5: UV-A light for 60 minutes.

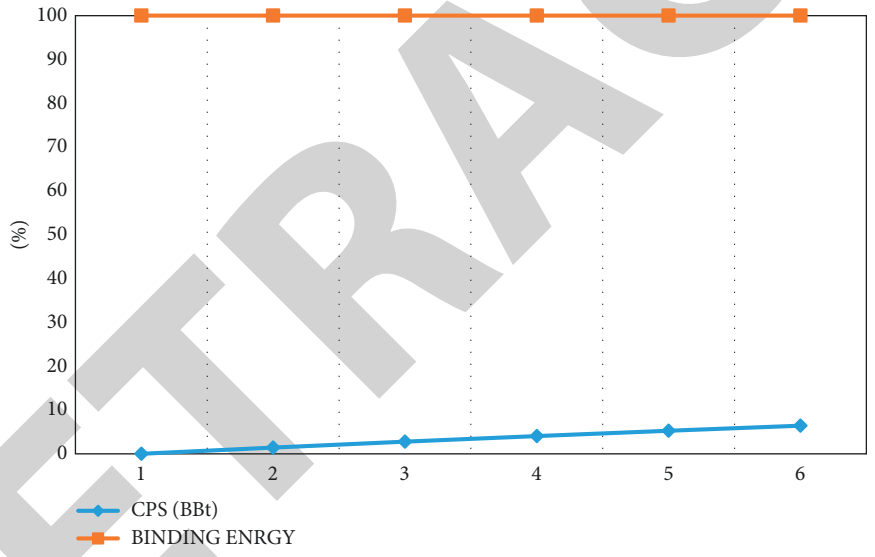


Figure 6: Apparent light for 3 hours.

harmony on the impetus surface, the combination was held under attractive blending in obscurity for an hour before openness to daylight. From then on, the entire arrangement was exposed to daylight with a normal power of 1.75 105 Lux units or 252.92 W/m$^2$ and an encompassing temperature of 35°C without changing the pH of the spouting. Moreover, the combination was reliably spinning at 150 rpm utilizing an engaging stirrer, and the mineralization of the shading iotas in the wastewater was assessed for six hours. Aliquots from the reactor were examined at different light time stretches (0 h, 1 h, 2 h, 3 h, 4 h, 5 h, and 6 h) prior to being centrifuged for 10 minutes at 12,000 rpm to eliminate any excess impetus [25]. This approach was then recreated with P-$WO_3$, I-$WO_3$, and I-P-$WO_3$ in comparable exploratory situations. Figure 7 shows the degradation efficiency of TOC in local dyeing wastewater by $WO_3$.

The photocatalytic decolorization of wastewater using undoped, monodoped, and codoped $WO_3$ nanoparticles was resolved using TOC and COD as pointer boundaries. The equation was used to determine the percentage of TOC.

$$EFFICIENCY\,(\%) = \frac{TOC0 - TOC1}{TOC0} \times 100, \quad (1)$$

$$EFFICIENCY\,(\%) = \frac{COD0 - COD1}{COD0} \times 100. \quad (2)$$

## 4. Result and Discussion

The physical-synthetic investigation of neighborhood colouring wastewater uncovered that marker values (TOC and

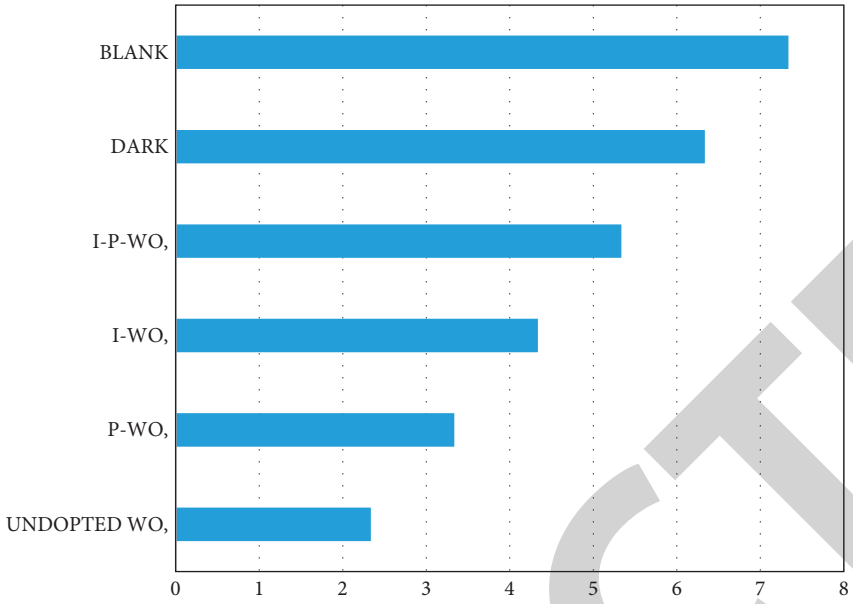


Figure 7: Degradation efficiency of TOC in local dyeing wastewater by $WO_3$.

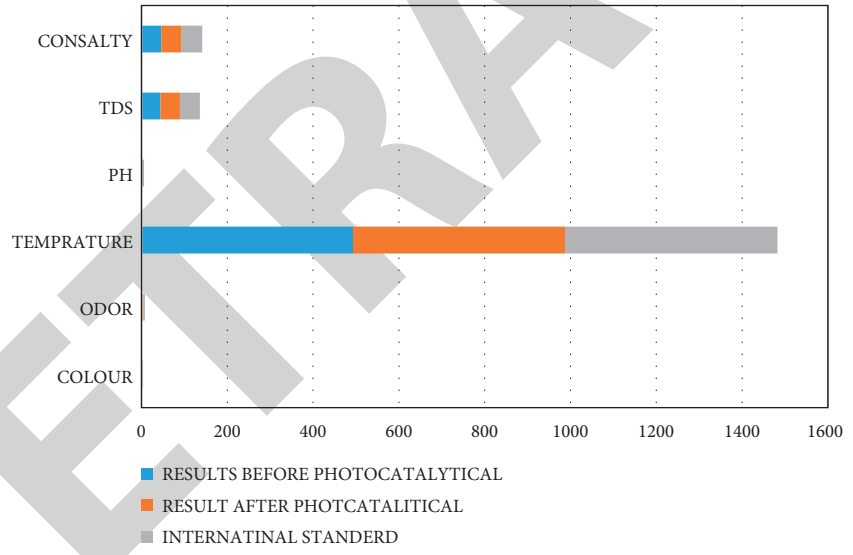


Figure 8: Physiochemical parameters of local dyeing wastewater from Kofar Mata dye pits, Kano.

COD) diminished following photocatalytic cooperation. The COD and TOC levels in crude wastewater are a lot more noteworthy because of the unnecessary utilization of natural colours and synthetic substances during colouring exercises. Strikingly, the BOD/COD proportion of roughly 0.37 uncovered the presence of an enormous number of nonbiodegradable normal tones. Figure 8 shows physiochemical parameters of local dyeing wastewater from Kofar Mata dye pits, Kano.

Subsequently, the untreated release of such organ phosphorus-doped tungsten trioxide poses a major enorgan challenge to human and aquatic animals alike [17, 26–28].

## 5. Conclusions

Tungsten oxide materials have acidic qualities (primarily Bronsted sites), an electrolyte, a high surface area (owing to the existence of oxygen vacancies), and a photostimulating effect when exposed to visible light, which are all advantageous for surface reactions and catalysis. The energy band gap of Woks is normally restricted to 2.6-2.8 eV for solidified $WO_3$ three-layered structures, but it can arrive at 5.5 eV for secluded $WO_4$ species (for example, bi-joined, di-oxo $WO_4$ carbon surface) or upheld Wok impetuses, contingent upon the stacking [17]. Each of these behaviors is customizable by

the operating circumstances of the catalyst. Centralizing structure and morphological characteristics (nanoplates, nanosheets, nanorods, nanowires, nanomesh, microflowers, hollow nanospheres, etc.), thermal treatment in a controlled environment, and connections with different mixtures (such as transmitters (carbon), semiconductors (e.g., $TiO_2$), and valuable metals); WOx particles can likewise be spread on substrates with a high explicit surface region. Based on these characteristics, $WO_3$-based impetuses for contamination expulsion have been made. One of the essential benefits of $WO_3$x's acidic and redox properties is their appropriateness for NOx reduction from fixed sources, especially $TiO_2$ and V2O5 (nitric corrosive plants first; treatment of incinerator and other ignition gases these days). Some VOCs are also reduced by using $WO_3$-based catalysts. Furthermore, surface oxygen vacancies can aid in the creation of gas sensors, particularly for the detection of $NO_2$. Sensitivity, selectivity, stability, repeatability, and reaction time can all be improved with modifications. Furthermore, there is a lot of interest in $WO_3$-based materials for photocatalysis applications in recent research. Due to the rapid recombination of photogenerated electrons and holes, bare $WO_3$ is not very active, but its photocatalytic activity can be considerably increased by a variety of associations [29]. $WO_3$-based photocatalysts are commonly used to degrade dyes, but they are also useful for treating wastewater contaminated with pharmaceutical compounds and plant protection goods. In the foreseeable future, this topic should continue to receive a lot of attention. [30–32].

The SO4 presence, the role of 2 anions, pH management in determining the last morphology, and the straightforward time of hydrothermally framed $WO_3$ nanostructures have been laid out. SO4 2 anions favored hexagonal nanobundle arrangements, though pH levels under 0.3 leaned toward the development of monoclinic-orthorhombic nanocubes. We assessed the impact of the shape and gem period of $WO_3$ on its capacity to photodegrade ethylene utilizing apparent light. Due to their unique geometric arrangement, the $WO_3$ nanocubes exhibit the best photodegradation capability.

## Data Availability

The data used to support the findings of this study are included within the article.

## Conflicts of Interest

The authors declare that they have no conflicts of interest.

## References


[1] O. M. Hussain, A. S. Swapnasmitha, J. John, and R. Pinto, "Structure and morphology of laser-ablated WO3 thin films," *Applied Physics A*, vol. 81, no. 6, pp. 1291–1297, 2005.

[2] S. K. Deb, "A novel electrophotographic system," *Applied Optics*, vol. 8, no. S1, p. 192, 1969.

[3] H. Kawasaki, TakeakiMatsunaga, W. Guan, T. Ohshima, Y. Yagyu, and J. Yoshiaki Suda, "Preparation of WO3 thin films for electrochromic display by plasma process," *Journal of Plasma and Fusion Research Series*, vol. 8, p. 1431, 2009.

[4] J. Huang, Y. Zhang, and Y. Ding, "Rationally designed/constructed $CoO_xWO_3$ anode for efficient photoelectrochemical water oxidation," *ACS Catalysis*, vol. 7, no. 3, pp. 1841–1845, 2017, [CrossRef].

[5] C.-G. Kuo, C.-Y. Chou, Ya-C. Tung, and J.-H. Chen, "Experimental Study of the electrochromic properties of WO3 thin films derived by electrochemical method," *Journal of Marine Science and Technology*, vol. 20, p. 365, 2012.

[6] B. M. Weckhuysen, J. M. Jehng, and I. E. Wachs, "In situ Raman spectroscopy of supported transition metal oxide Catalysts: $^{18}O_2$–$^{16}O_2$ isotopic labeling studies," *Journal of Physical Chemistry B*, vol. 104, no. 31, pp. 7382–7387, 2000.

[7] X. Li, X.-S. Li, J. Chen, J. Li, and J. Hao, "An efficient novel regeneration method for Ca-poisoning V2O5-WO3/TiO2 catalyst," *Catalysis Communications*, vol. 87, pp. 45–48, 2016, [CrossRef].

[8] X. Li, X. S. Li, R. T. Yang, J. Mo, J. Li, and J. Hao, "The poisoning effects of calcium on V2O5-WO3/TiO2 catalyst for the SCR reaction: comparison of different forms of calcium," *Molecular Catalysis*, vol. 434, pp. 16–24, 2017, [CrossRef].

[9] C. I. Odenbrand, "CaSO4 deactivated V2O5 -WO3/TiO2 SCR catalyst for a diesel power plant. Characterization and simulation of the kinetics of the SCR reactions," *Applied Catalysis B: Environmental*, vol. 234, pp. 365–377, 2018, [CrossRef].

[10] H. H. Phil, M. P. Reddy, P. A. Kumar, L. K. Ju, and J. S. Hyo, "SO2 resistant antimony promoted V2O5/TiO2 catalyst for NH3 -SCR of NOx at low temperatures," *Applied Catalysis B: Environmental*, vol. 78, no. 3-4, pp. 301–308, 2008, [CrossRef].

[11] D. W. Kwon, K. H. Park, and S. C. Hong, "Enhancement of SCR activity and SO2 resistance on VOx/TiO2 catalyst by addition of molybdenum," *Chemical Engineering Journal*, vol. 284, pp. 315–324, 2016, [CrossRef].

[12] M. Fumiaki, H. Eiichi, I. Tomoaki, K. Ebihara, and T. Raj Kumar, "WO3 thin films prepared by pulsed laser deposition," *Journal of Applied Physics*, vol. 41, p. 5372, 2002.

[13] K. Gesheva, A. Cziraki, T. Ivanova, and A. Szekeres, "Thermally induced structural transformations in CVD transition metal oxide thin films," *Journal of Optoelectronics and Advanced Materials*, vol. 7, no. 1, p. 557, 2005.

[14] A. C. Argun and J. R. Reynolds, "The first truly all-polymer electrochromic devices," *Journal of Advanced Materials*, vol. 15, p. 1338, 2003.

[15] M. B. Alazzam and F. Alassery, "The dynamic movement of disaster management systems based on vehicle networks and applied on the healthcare system," *Applied Bionics and Biomechanics*, vol. 2021, Article ID 5710294, 8 pages, 2021.

[16] H. Li, J. Miao, Q. Su, Y. Yu, Y. Chen, and J. Chen, "SCR catalysts modified by Ce and Cu," *Journal of Materials Science*, vol. 54, pp. 14707–14719, 2019, [CrossRef].

[17] T. Xu, X. Wu, Y. Gao, Q. Lin, J. Hu, and D. Weng, "Comparative study on sulfur poisoning of V2O5-Sb2O3/TiO2 and V2O5-WO3/TiO2 monolithic catalysts for low-temperature NH3-SCR," *Catalysis Communications*, vol. 93, pp. 33–36, 2017, [CrossRef].

[18] N. Zhu, W. Shan, Z. Lian, Y. Zhang, K. Liu, and H. He, "A superior Fe-V-Ti catalyst with high activity and SO2 resistance for the selective catalytic reduction of NO with NH3," *Journal of Hazardous Materials*, vol. 382, pp. 120970–120978, 2020, [CrossRef].

[19] S. Rajagopal, D. Nataraj, D. Mangalaraj, D. Yahia, R. Jacques, and O. Yu. Khyzhun, "Controlled growth of WO3nanostructures with three different morphologies and their structural, optical, and photodecomposition studies," *Nanoscale Research Letters*, vol. 4, p. 1335, 2009.

[20] Y. Li, W. Zhang, and B. Qiu, "Enhanced surface charge separation induced by Ag nanoparticles on WO3 photoanode for photoelectrochemical water splitting," *Chemistry Letters*, vol. 49, no. 6, pp. 741–744, 2020, [CrossRef].

[21] L. Xu, C. Wang, H. Chang, Q. Wu, T. Zhang, and J. Li, "New insight into SO2 poisoning and regeneration of CeO2 -WO3/TiO2 and V2O5 -WO3/TiO2 catalysts for low-temperature NH3 -SCR," *Environmental Science and Technology*, vol. 52, no. 12, pp. 7064–7071, 2018, [CrossRef].

[22] A. Hameed, M. Gondal, and Z. Yamani, "Effect of transition metal doping on photocatalytic activity of WO3 for water splitting under laser illumination: role of 3D-orbitals," *Catalysis Communications*, vol. 5, no. 11, pp. 715–719, 2004, [CrossRef].

[23] A. Enesca, A. Duta, and J. Schoonman, "Study of photoactivity of tungsten trioxide (WO3 ) for water splitting," *Thin Solid Films*, vol. 515, no. 16, pp. 6371–6374, 2007, [CrossRef].

[24] R. A. Pala, A. J. Leenheer, M. Lichterman, H. A. Atwater, and N. S. Lewis, "Measurement of minority-carrier diffusion lengths using wedge-shaped semiconductor photoelectrodes," *Energy & Environmental Science*, vol. 7, no. 10, pp. 3424–3430, 2014, [CrossRef].

[25] R. H. Coridan, K. A. Arpin, B. S. Brunschwig, P. V. Braun, and N. S. Lewis, "Photoelectrochemical behavior of hierarchically structured Si/WO3 core–shell tandem photoanodes," *Nano Letters*, vol. 14, no. 5, pp. 2310–2317, 2014, [CrossRef].

[26] Y. Wang, H. Shi, K. Cui, L. Zhang, S. Ge, and J. Yu, "Reversible electron storage in tandem photoelectrochemical cell for light driven unassisted overall water splitting," *Applied Catalysis B: Environmental*, vol. 275, Article ID 119094, 2020[CrossRef].

[27] O. S. Ahmed, E. E. Omer, S. Z. Alshawwa, M. B. Alazzam, and R. A. Khan, "Approaches to federated computing for the protection of patient privacy and security using medical applications," *Applied Bionics and Biomechanics*, vol. 2022, Article ID 1201339, 6 pages, 2022.

[28] J. Jun, S. Ju, S. Moon et al., "The optimization of surface morphology of Au nanoparticles on WO3 nanoflakes for plasmonic photoanode," *Nanotechnology*, vol. 31, no. 20, Article ID 204003, 2020[CrossRef].

[29] W. T. Mohammad, S. H. Mabrouk, R. M. A. E. Mostafa et al., "Artificial intelligence technique of synthesis and characterizations for measurement of optical particles in medical devices," *Applied Bionics and Biomechanics*, vol. 2022, Article ID 9103551, 5 pages, 2022.

[30] S. L. Wang, Y. L. Mak, S. Wang et al., "Visible–near-infrared-light-Driven oxygen evolution reaction with noble-metal-free WO2–WO3 hybrid nanorods," *Langmuir*, vol. 32, no. 49, pp. 13046–13053, 2016, [CrossRef] [PubMed].

[31] J. H. Baek, B. J. Kim, G. S. Han et al., "BiVO4/WO3/SnO2 Double-Heterojunction photoanode with enhanced charge separation and visible-transparency for bias-free solar water-splitting with a perovskite solar cell," *ACS Applied Materials and Interfaces*, vol. 9, no. 2, pp. 1479–1487, 2017, [CrossRef].

[32] S. W. Tsai and H. T. Hahn, *Introduction to Composite Materials*, Routledge, Oxfordshire, UK, 2018.